PROCEEDINGS A

royalsocietypublishing.org/journal/rspa

Research

Cite this article: Andrews B, Möller G. 2023 Self-similarity of spectral response functions for fractional quantum Hall states. *Proc. R. Soc. A* **479**: 20230021. https://doi.org/10.1098/rspa.2023.0021

Received: 11 January 2023
Accepted: 20 June 2023

Subject Areas:
quantum physics, solid-state physics, statistical physics

Keywords:
fractional quantum Hall effect, spectral response functions, dynamical structure factors, self-similarity, fractals

Author for correspondence:
Bartholomew Andrews
e-mail: bandrews@berkeley.edu

Electronic supplementary material is available online at https://doi.org/10.6084/m9.figshare.c.6742498.

THE ROYAL SOCIETY PUBLISHING

Self-similarity of spectral response functions for fractional quantum Hall states

Bartholomew Andrews[1,2,3] and Gunnar Möller[4]

[1]Department of Physics, University of Zurich, Winterthurerstrasse 190, Zurich 8057, Switzerland
[2]Department of Physics and Astronomy, University of California at Los Angeles, 475 Portola Plaza, Los Angeles, CA 90095, USA
[3]Department of Physics, University of California at Berkeley, 100 South Drive, Berkeley, CA 94720, USA
[4]Physics and Astronomy, Division of Natural Sciences, University of Kent, Ingram Building, Canterbury CT2 7NZ, UK

BA, 0000-0002-9079-7433; GM, 0000-0001-8986-0899

Spectral response functions are central quantities in the analysis of quantum many-body states, since they describe the response of many-body systems to external perturbations and hence directly correspond to observables in experiments. In this paper, we evaluate a momentum-averaged dynamical density structure factor for the fermionic $\nu = 1/3$ fractional quantum Hall (FQH) state on a torus, using the continued fraction method to compute the dynamical correlation function. We establish the scaling behaviour of the screened Coulomb structure factor with respect to interaction range, and expose an inherent self-similarity of structure factors in the frequency domain. These results highlight the statistical properties of spectral response functions for FQH states and show how they can be efficiently approximated in numerical models.

1. Introduction

One of the key observables yielding insights into interacting quantum systems is the dynamical structure factor $S(\mathbf{q}, \omega)$, which captures the complete momentum- and energy-resolved spectrum of particle excitations. Apart from its central role in the dynamics of quantum many-body systems, the structure factor has

a number of appealing properties that stimulate a broad range of research. In particular, we focus on its application in fractional quantum Hall (FQH) systems, which have been known for several decades to host a rich spectrum of collective modes [1–4], and have been extended to both lattice models [5,6] and effective field theories [7,8]. Since the structure factor is directly related to the correlation function, it can be computed in a variety of ways, such as via Feynman diagram resummation [3] or continued fractions [9]. Moreover, the structure factor can be directly probed in two-dimensional electron gases, e.g. via surface acoustic waves [10,11], and analysed using Raman scattering to reveal additional spin properties [12]. Despite its rich structure and experimental applicability, however, numerical studies that systematically investigate the spectral response of FQH states have only recently gained traction [5,8,13–17].

In this paper, we study a type of dynamical density structure factor[1] for the $\nu = 1/3$ fermionic Laughlin state on a torus, using the continued fraction method to compute the dynamical correlation function. In particular, two aspects of the structure factor are investigated: (i) the effect of interaction range and (ii) self-similarity. We start by tuning between the V_1 and screened Coulomb interactions to reveal the scaling behaviour of the structure factor with respect to interaction range. Then, motivated by the fractality of continued fraction Green's functions [19,20], we study the self-similarity of structure factors for long-range interactions in the frequency domain. In both cases, we present systematic exact diagonalization computations, which we scale with system size. Our results expose the scaling behaviour of the structure factor with respect to interaction range, which reflects the functional form of the interaction. Moreover, we reveal that FQH dynamical structure factors are statistically self-similar fractals in the frequency domain, across several orders of magnitude. Apart from providing a deeper insight into the spectral properties of FQH systems, these results may be exploited to compute response functions more efficiently.

The outline of the paper is as follows. In §2, we define our FQH system, and in §3, we describe the method for computing and analysing the structure factors. Subsequently, in §4, we present our exact diagonalization results. In §4a, we tune the structure factors between the V_1 and Coulomb interactions and study the effect of screening. In §4b, we examine the self-similarity of the Coulomb structure factor as the frequency domain is rescaled. Finally, in §5, we discuss the implications with respect to future numerical investigations.

2. Model

We consider a two-dimensional system of N_f spin-polarized fermions of mass m_f and charge q_f in a perpendicular magnetic field B on the xy-plane with periodic boundary conditions. Building on earlier work [4,21–23], the torus geometry has recently experienced a revival of interest [5,6,24–29], which motivates our choice. We consider the Landau gauge such that the momentum k_y is a good quantum number. The energy spectrum of this FQH set-up is split into Landau levels, the lowest of which we fill up to a filling factor $\nu = N_f/N_\Phi$, where N_Φ is the number of flux quanta in the system. Moreover, we focus on the regime where the interaction is weak compared with the Landau level spacing (given by the cyclotron frequency $\omega_c = q_f B/m_f$). Hence, to a good approximation, we may project the interaction Hamiltonian to the lowest Landau level (LLL), such that

$$H = H_{\text{kin}} + \sum_{i<j}^{N_f} P_{\text{LLL}} V(|\mathbf{r}_i - \mathbf{r}_j|) P_{\text{LLL}}, \tag{2.1}$$

where H_{kin} is the constant kinetic part of the Hamiltonian, P_{LLL} is the LLL projection operator, V is the interaction potential and $\mathbf{r}_i$ is the displacement of particle i. The relevant length scale in the problem is the magnetic length $l_B = 1/\sqrt{q_f B}$.

[1]We note that the dynamical density structure factor is also known as the density-density response function [18] or spectral function of the density operator [8] in related works.

In this paper, we consider the Coulomb $V^C(r) \sim r^{-1}$ and Yukawa $V^Y_\lambda(r) \sim r^{-1}\,\mathrm{e}^{-\lambda r}$ interactions explicitly by diagonalizing the Hamiltonian directly in Fourier space, where λ is the Yukawa mass. However, we note that it is not always necessary or desirable to directly account for a long-range interaction in this way. Haldane showed that for systems with a translation and rotation invariant two-body interaction, the interaction Hamiltonian may be written as

$$H_{\mathrm{int}} = \sum_{i<j} \sum_{L} V_L P^L_{ij}, \tag{2.2}$$

where V_L are the Haldane pseudopotentials, L is the relative angular momentum quantum number between particles i and j, and P^L_{ij} is the corresponding projection operator. This simplifies a certain class of long-range interactions into a simple sum of projectors, which has found a diverse set of applications from accelerating early numerical computations on the sphere, through to modelling realistic semiconductor heterojunctions [24]. Consequently, we complement our analysis by using a Haldane pseudopotential formalism in Sec. SI of the electronic supplementary material.

Throughout our study, we focus on the primary Laughlin state defined at the filling factor $\nu = 1/3$. Laughlin famously proposed a wave function ansatz for the ground state of a FQH system with particles interacting via the Coulomb potential in a $1/m$-filled LLL, where m is an odd integer. Although the Laughlin ansatz is a successful description of the problem, since it is in the correct universality class, it is not the exact ground state for the Coulomb interaction. Rather, it was later shown to be the unique, highest-density, zero-energy state for the V_1 Haldane pseudopotential. In this paper, we investigate the $\nu = 1/3$ state in both limits. When we discuss the 'Laughlin state', we refer to the general ground state solution to a FQH system with a $1/m$-filled LLL and not the Laughlin ansatz wave function, in particular.

3. Method

In this section, we outline our numerical method. In §3a, we introduce the continued fraction algorithm for computing dynamical structure factors and in §3b, we define fractals and self-similar distributions.

(a) Structure factors

In order to efficiently find the eigenspectrum of the many-body Hamiltonian in equation (2.1), we employ the Lanczos algorithm [9]. This method uses an orthogonal Krylov basis, in which the original Hamiltonian H is transcribed to a tridiagonal form $\check{H}$, to compute the eigenbasis

$$H\,|\Psi_i\rangle = E_i\,|\Psi_i\rangle \quad \text{with } i = 0, \ldots, N-1 \tag{3.1}$$

and

$$\check{H}\,|\check{\Psi}_j\rangle = \check{E}_j\,|\check{\Psi}_j\rangle \quad \text{with } j = 0, \ldots, M-1, \tag{3.2}$$

where the check marks denote the Krylov representation, N is the dimension of the original Hamiltonian H and $M \leq N$ is the dimension of the Lanczos Hamiltonian $\check{H}$. Tridiagonlization in the Krylov space is rapid, since many degrees of freedom are simultaneously used in the optimization, and memory efficient, since only two vectors of length N need to be stored.[2] Moreover, there is typically good agreement between extremal eigenvalues in the Krylov representation $\check{E}_j$ and those in the original system E_i, even for $M \ll N$ [9,30,31]. Further details of the method are presented in Sec. SII of the electronic supplementary material.

The Lanczos algorithm was later extended by Haydock *et al.* and applied to compute observables in physical systems with a large number of particles [32–37]. In particular, Haydock showed that the resolvent of the Hamiltonian can be efficiently computed using a continued fraction expansion, which is useful for calculating local quantities, such as the single-particle

[2]An additional third vector may be stored to restart the algorithm from a specific point.

density matrix and the density of states. Crucially, when the original Hamiltonian H is written as a tridiagonal Hamiltonian $\check{H}$ in the Krylov basis, the problem is effectively reduced to a chain of length M, which expedites the computation. The algorithm is consequently a widely used approach in large-scale exact diagonalization computations for quantum many-body systems and has been optimized to diagonalize sparse matrices as large as $\dim(H) \sim 10^9$ [38–40].

For our system, we work in momentum space and consider the zero-temperature dynamical correlation function for the operator $O_{\mathbf{q}}$ in the Lehmann representation, which using the Krylov basis may be approximated as

$$\check{G}_O(\mathbf{q}, z) = \sum_{j=0}^{M-1} \frac{|\langle \check{\Psi}_j | O_{\mathbf{q}} | \Psi_0 \rangle|^2}{E_0 + z - \check{E}_j} \tag{3.3}$$

$$= \langle \Psi_0 | O_{\mathbf{q}}^\dagger \frac{1}{E_0 + z - \check{H}} O_{\mathbf{q}} | \Psi_0 \rangle \,, \tag{3.4}$$

where $\mathbf{q} \equiv (q_x, q_y)$ are the Fourier components of the O operator, $z \equiv \omega + \mathrm{i}\epsilon$, ω is the frequency and ϵ is a small parameter used to avoid poles in the expansion. From this formula, it is straightforward to show that for the symmetric tridiagonal Hamiltonian $\check{H}$, with $(b_j)a_j$ along the (sub)diagonal, the correlation function may be written as a continued fraction

$$\check{G}_O(\mathbf{q}, z) = \frac{\langle \Psi_0 | O_{\mathbf{q}}^\dagger O_{\mathbf{q}} | \Psi_0 \rangle}{E_0 + z - a_0 - b_1^2/(E_0 + z - a_1 - b_2^2/\ldots)}, \tag{3.5}$$

which terminates at $-b_{M-1}^2/(z - a_{M-1})$. This form of the correlation function converges rapidly to machine precision [31].

Specifically, we focus on the density-density correlation functions arising from the density operator

$$\rho_{\mathbf{q}} \equiv \int \mathrm{d}\mathbf{r}\, \mathrm{e}^{\mathrm{i}\mathbf{q}\cdot\mathbf{r}} c^\dagger(\mathbf{r}) c(\mathbf{r}), \tag{3.6}$$

where $\mathbf{r} \equiv (x, y)$ is the position operator conjugate to $\mathbf{q}$. Given our choice of Landau gauge with definite momentum k_y, we are particularly interested in resolving the q_y Fourier components of the density operator. We therefore choose to integrate out the q_x modes on the torus to avoid an additional free variable and consider the q_x-momentum-averaged density operator, setting

$$O_{q_y} \equiv \bar{\rho}_{q_y} = \sum_{m=0}^{N_\Phi - 1} \rho_{q_x = (2\pi m / L_x), q_y}, \tag{3.7}$$

where $L_x \times L_y$ are the system dimensions. We have separately verified, by evaluating at specific q_x values, that the density operator is only weakly dependent on q_x. The full derivation of the momentum-averaged density operator is presented in Sec. SIII of the electronic supplementary material. Finally, we may use this operator to compute the corresponding dynamical density structure factor

$$\check{I}_{\bar{\rho}}(q_y, \omega) = -\frac{1}{\pi} \lim_{\epsilon \to 0} \mathrm{Im}\, \check{G}_{\bar{\rho}}(q_y, \omega + \mathrm{i}\epsilon), \tag{3.8}$$

which we often refer to simply as the 'structure factor'. The crucial property of the continued fraction expansion is that the structure factor in the Krylov representation $\check{I}$ accurately reproduces the moments of the structure factor in the Hilbert representation I, and so we now drop the check marks [9].

(b) Fractals and self-similarity

In this work, we investigate the self-similarity of the structure factors $I_{\bar{\rho}}(q_y, \omega)$. Fractals and self-similarity appear in many contexts in condensed matter physics, such as the Hofstadter spectrum of energy levels for electrons hopping in a periodic potential [41], the Haldane hierarchy of stable

FQH filling fractions [42], and the statistical analysis of time series [43]. Moreover, they have several important characteristics that can often be leveraged in theory and simulations.

A fractal is defined as an object with a fractal dimension D that is greater than its topological dimension d [44]. The fractal dimension may be computed in a variety of ways, however is traditionally defined via $n \equiv s^{-D}$, where n is the number of units in the whole object and s is the scale factor. One of the distinctive properties of fractals is their scale-invariance, also known as self-similarity, where subregions of a structure are identical to the whole. However, we note that not all self-similar objects are fractals. For example, a square is a self-similar object with $D = d = 2$, whereas a Koch curve is a fractal with $D = \log(4)/\log(3) > d$ [45].

As for the fractional dimension above, self-similarity may also be defined differently depending on the context. Exact self-similarity holds on all scales, and in this case the various definitions of the fractal dimension coincide. However, quasi- or multi-fractal self-similarity is more common, with lower and upper bounds on where this behaviour applies. In functional analysis, self-similarity occurs when a subsection of a function statistically resembles the entire function. Specifically, for a function of one variable $I(\omega)$, this occurs when

$$I(\omega) \equiv s^{\kappa} I\left(\frac{\omega}{s}\right), \tag{3.9}$$

where s is a scale factor and κ is the self-similarity parameter [46]. In equation (3.9), '$\equiv$' implies that the distributions on both sides of the equation are statistically identical. However, in practice, this is approximated by examining the first and second moments [46–48].

In contrast to geometric analysis, a general function of one variable is in a two-dimensional space where each axis represents different physical quantities. Consequently, two magnification factors are required to quantify self-similarity, such that

$$\kappa \equiv \frac{\log M_y}{\log M_x}, \tag{3.10}$$

where M_i is the magnification factor of the i-axis. Note that this takes an analogous form to the definition of fractal dimension discussed above, albeit with a different interpretation. The fractional dimension of a function is often difficult to quantify. However, since the demonstration of self-similarity for any non-trivial curve indicates detail across many orders of magnitude, which precludes an integer dimension, this is taken as evidence to show that a curve is a fractal with respect to the axes on which the magnification occurs.

4. Results

In this section, we present our exact diagonalization results [49]. In §4a, we investigate the scaling of structure factors as we tune from the V_1 to the screened Coulomb interaction, and in §4b, we expose a statistical self-similarity of structure factors in the frequency domain.

(a) Tuning the interaction range

We compute the momentum-averaged dynamical density structure factor $I_{\tilde{\rho}}$ for the $\nu = 1/3$ Laughlin state stabilized by a linear superposition of the V_1 Haldane pseudopotential [42] and an explicit $V_\lambda^Y(q)$ Yukawa interaction. In this system, the interaction Hamiltonian is given as $H_{\text{int}} = (1-\alpha)H_{V_1} + \alpha H_{V_\lambda^Y}$, where $\alpha \in [0, 1]$. The tuning parameter α allows us to interpolate between two common ground state solutions in the same universality class, and the Yukawa mass λ enables us to vary the interaction range and recover the Coulomb limit.

In figure 1*a*,*b*, we start by computing the structure factors corresponding to the two most common approaches for stabilizing the $\nu = 1/3$ Laughlin state, via the V_1 and Coulomb interactions. We present our initial results for all q_y momentum sectors. Since the structure factor defined in equation (3.8) conserves particle number, these plots show the coupling of the ground state to gapped excitations and consist of a spectrum of peaks at finite frequency. As expected: the structure factor corresponding to the V_1 interaction yields a broader spread of frequencies, due to

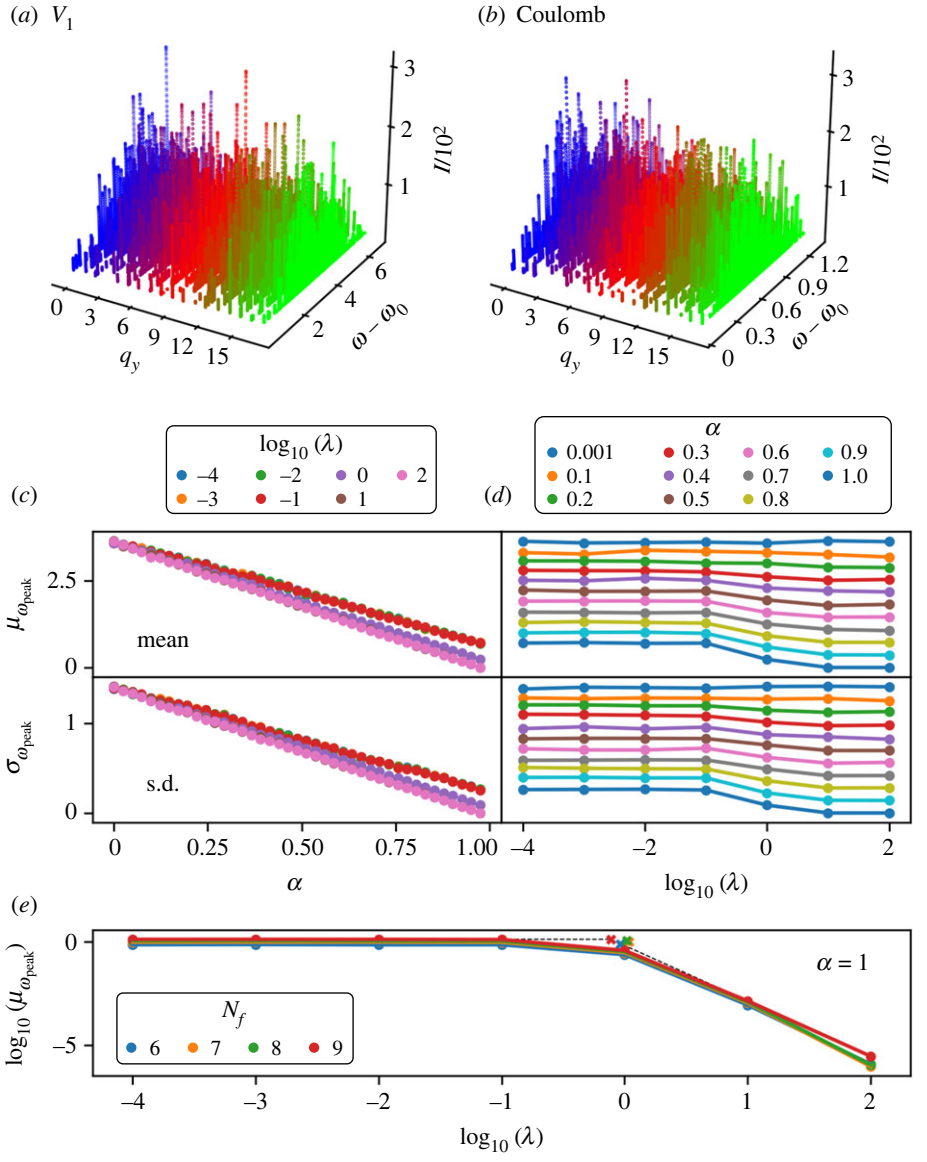

Figure 1. Tuning the structure factor with respect to interaction range. Structure factors $I_{\bar{\rho}}(q_y, \omega)$ as a function of angular frequency offset by the ground state energy $\omega - \omega_0$, for the $\nu = 1/3$ FQH state on a torus, with $N_f = 6$ particles and $N_\Phi = 18$ flux quanta, stabilized by (*a*) the $V_1 = 1$ pseudopotential, (*b*) the exact Coulomb interaction V^C and (*c–e*) $H_{\text{int}} = (1 - \alpha)H_{V_1} + \alpha H_{V_\lambda^\gamma}$, in the LLL. In (*a*,*b*), the spectra are resolved with respect to their q_y momentum sector, whereas in (*c–e*) $q_y = 0$. The mean, μ, and standard deviation, σ, of offset angular frequencies coinciding with spectral peaks, ω_{peak}, are shown as a function of (*c*) α and (*d*) λ. (*e*) Finite-size scaling of the $\alpha = 1$ curve from (*d*). The transition points between the two regimes are marked with crosses. The computations were performed with a resolution of (*a*,*b*) $\Delta\omega = 10^{-5}$, $\Delta I = 10^{-5}$, $\epsilon = 10^{-4}$ and (*c–e*) $\Delta\omega = 10^{-7}$, $\Delta I = 10^{-4}$, $\epsilon = 10^{-6}$.

the normalization of the $V_1 = 1$ pseudopotential [14]; the relative peak amplitudes are consistent in the two cases, owing to the dominant V_1 component of the Coulomb interaction [13,16]; and the shape of both distributions is unimodal, according to the theory for Laughlin states.[3] Up to

[3]In the literature, these collective peaks are typically q_x-momentum-resolved and may sometimes be referred to simply as peaks [14,15], or collective modes [13,16] in certain contexts.

slight variations in the number and heights of the peaks, the overall shape of the envelope holds for all runs and for all q_y, and there is a close resemblance between the structure factors of these two FQH states.

Motivated by the effect that interaction range has on the form of the structure factors, in figure 1*c*,*d*, we tune $I_{\tilde{\rho}}(0,\omega)$ from figure 1*a*,*b*, with respect to α and λ, at the increased resolution of $\Delta\omega = 10^{-7}$ and $\epsilon = 10^{-6}$.[4] We note that decreasing ϵ has the auxiliary effect of proportionally increasing the peak amplitudes and decreasing the peak widths. We present the evolution of the first two moments of the distribution: the mean (top panels) and standard deviation (bottom panels). In this case, we consider the offset angular frequencies coinciding with spectral peaks, ω_{peak}, and use their mean, $\mu_{\omega_{\text{peak}}}$, and standard deviation, $\sigma_{\omega_{\text{peak}}}$, as quantifiers of centre and spread, respectively.[5]

From the constant gradient of the first two moments in figure 1*c*, we can see that the structure factor scales linearly with the tuning parameter α. This is expected, since we are effectively multiplying the Yukawa interaction by a scale factor modulo a correction from the V_1 term. Subsequently, in figure 1*d*, we plot the scaling of the structure factor on different axes, to clearly show the influence of λ. As $\alpha \to 0$, the structure factor does not depend on λ, since there is a vanishing component of the Yukawa interaction in the Hamiltonian. Similarly, the influence of λ increases linearly with α. Most notably, however, we observe two non-trivial scaling regimes for the structure factor as $\alpha \to 1$. For $\log\lambda \lesssim -1$, the structure factor is approximately independent of λ, whereas for $\log\lambda > -1$, the centre and spread exponentially diminish to zero. This behaviour reflects the exponential suppression of the Yukawa interaction potential at large Yukawa mass, which correspondingly restricts the domain of the response functions.

To investigate this transition in detail, in figure 1*e*, we illustrate the finite-size scaling of the $\alpha = 1$ curve from the top panel of figure 1*d* on a log-log plot. Here, we see explicitly that the continuous connection between α and λ translates to a non-trivial scaling with respect to λ, with two regimes. Connecting lines of best fit from these two regions yields a transition point at $\log\lambda \approx 0$. Using equation (3.10), with M_x corresponding to λ and M_y corresponding to $\mu_{\omega_{\text{peak}}}$, we obtain the self-similarity parameters $\kappa_\mu = 0.00116$ and -2.67 for $\log\lambda \lesssim 0$ and $\log\lambda > 0$, respectively. This reflects the asymptotic scaling of the Yukawa interaction potential in the small and large λ limits. Note that we used a linear scale for α in figure 1*c*, since this corresponds to linearly interpolating between two Hamiltonians, whereas we use a logarithmic scale for λ, to analyse a wide scope of interaction ranges.[6]

In this section, we have established the scaling of structure factors with respect to α and λ in the framework of statistical self-similarity, and showed that it reflects the functional form of the interaction. Moreover, the scaling is not *exactly* self-similar, since the combined effect of peak fluctuations due to microscopic details of the Hamiltonian, and numerical noise due to sample aliasing, yields approximately 1% fluctuations in peak number and amplitude.

(b) Rescaling the frequency domain

Previously, we demonstrated that the structure factor scales trivially with respect to a linear interpolation between the V_1 and screened Coulomb interactions, and non-trivially with respect to interaction range, reflecting the functional form of the interaction. In both cases, this scaling is the result of tuning parameters; namely, α and λ. In this section, we investigate a form of self-similarity with respect to the frequency domain, which cannot be explicitly linked to a tuning parameter.

In figure 2, we investigate the distribution of the peak magnitudes, I_{peak}, in the Coulomb structure factor from figure 1*b*, as we scale the frequency domain. For clarity, we denote

[4]Although the evolution is shown only for $q_y = 0$, this analysis holds for all momentum sectors.

[5]In figure 1, we chose to study the self-similarity of $\{\omega_{\text{peak}}\}$ with respect to the α and λ axes. However, analogous relations also hold for $\{I_{\text{peak}}\}$.

[6]The interaction matrix elements are too small for $\lambda \geq 10^3$ to reliably stabilize the fermionic Laughlin state.

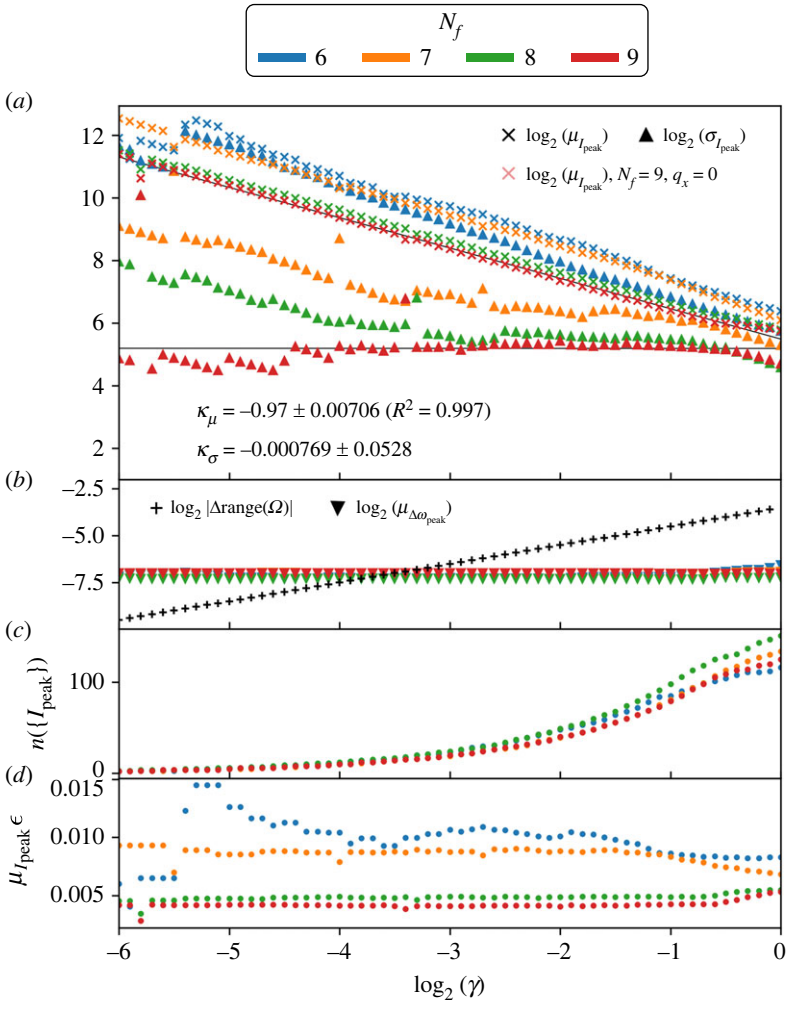

Figure 2. Rescaling the structure factor in the frequency domain. Structure factor $I_{\bar{\rho}}(0, \omega)$ for the $\nu = 1/3$ FQH state on a torus, with $N_f = 6, 7, 8, 9$ particles, stabilized by the exact Coulomb interaction V^C, in the LLL. For comparison, we overlay the $N_f = 9$ data at $q_x = 0$ with half opacity. (*a*) Mean, μ, and standard deviation, σ, of the peaks of the structure factor, I_{peak}, as we symmetrically scale the Ω_0 domain about its midpoint $\omega_{\text{mid}} = (\omega_{\text{min}} + \omega_{\text{max}})/2$, by a scale factor $\gamma \equiv \text{range}(\Omega)/\text{range}(\Omega_0)$. The initial frequency domain, Ω_0, is chosen to span the entire structure factor. For each iteration, we correspondingly scale ϵ, to reduce the widths of the peaks, and $\Delta\omega$ to increase our numerical resolution. The lines of best fit for the $N_f = 9$ data in the linear regions are drawn in black and the self-similarity parameters are given by the gradients of the slopes. (*b*) The magnitude of the Ω domain reduction between successive steps, $\Delta\text{range}(\Omega_i) \equiv \text{range}(\Omega_i) - \text{range}(\Omega_{i-1})$, where i is the frequency domain index, and the average separation between ω_{peak} values, $\mu_{\Delta\omega_{\text{peak}}}$. (*c*) The number of peaks, $n(\{I_{\text{peak}}\})$, and (*d*) the average peak magnitude, $\mu_{I_{\text{peak}}}$, as we scale Ω. The first computation with $\Omega = \Omega_0$ was performed with a resolution of $\Delta\omega = 10^{-5}$, $\Delta I = 10^{-5}$ and $\epsilon = 10^{-4}$.

angular frequencies with a lower-case ω and a set of angular frequencies with an upper-case $\Omega \equiv \{\omega\}$. We consider an initial frequency domain Ω_0 with $\text{range}(\Omega_0) = \omega_{\text{max}} - \omega_{\text{min}}$, which we scale symmetrically about its midpoint $\omega_{\text{mid}} = (\omega_{\text{min}} + \omega_{\text{max}})/2$, by a scale factor $\gamma \equiv \text{range}(\Omega)/\text{range}(\Omega_0)$. We choose Ω_0 to span the entire structure factor, although we note that the precise choice is arbitrary. In order to keep the scaling numerically consistent, we correspondingly scale the frequency resolution, $\Delta\omega$, and the ϵ value in our simulations. In figure 2*a*, we plot the first two moments of the distribution against the domain scale factor to

compute the self-similarity parameters. We additionally scale this with system size up to $N_f = 9$ particles. We find that there is a contiguous linear region, which grows with system size, and has a correlation coefficient of $R^2 > 0.99$,[7] which indicates a statistical self-similarity of the Coulomb structure factor with respect to frequency domain rescaling. This behaviour also holds for the q_x-momentum-resolved dynamical density structure factor, as demonstrated for $N_f = 9$, $q_x = 0$. The self-similarity parameters for the mean and standard deviation are $\kappa_\mu = -0.97 \pm 0.00706$ and $\kappa_\sigma = -0.000769 \pm 0.0528$. As mentioned in §4a, since a reduction of ϵ increases the heights of the peaks, it is consistent that the self-similarity parameter $\kappa_\mu \approx -1$. Finite-size scaling shows that the self-similarity parameter for the standard deviation holds deeper into the domain rescaling procedure with increasing system size, and maintains a constant value across the entire procedure for $N_f = 9$, up to sampling effects at small Ω. In figure 2*b*, we compare the magnitude of the frequency interval reduction between successive steps, $\Delta\text{range}(\Omega_i) \equiv \text{range}(\Omega_i) - \text{range}(\Omega_{i-1})$, where i is the frequency domain index, with the average spacing between the peaks, $\mu_{\Delta\omega_{\text{peak}}}$. Since the frequency domain scaling requires a finite section of structure factor peaks to be truncated on each iteration, this allows us to verify the continuity of the procedure. We observe that the average spacing between the peaks is initially smaller than the size of the frequency interval being removed, up to $\gamma \approx 2^{-3.5}$. For smaller values of γ, breakdowns in the rescaling continuity become more likely, as observed for the $\sigma_{I_{\text{peak}}}$, $N_f = 9$ data in figure 2*a*. However, the average spacing between the peaks remains constant, independent of particle number, which shows that this is not the cause of numerical breakdown for small system sizes. In figure 2*c*, we examine the number of peaks in the structure factor, $n(\{I_{\text{peak}}\})$, with frequency domain rescaling. Since the moments of a distribution are sensitive to the sample size, this is another validity test for the self-similar scaling. We find that the number of peaks in the structure factor decreases exponentially with frequency domain reduction, which holds independently of system size, up to the influence of initial conditions at $\Omega \approx \Omega_0$. Nevertheless, for $\gamma \lesssim 2^{-5.5}$, we find that for smaller particle numbers, there are slightly fewer peaks in the spectrum, which may be a contributing cause of the numerical breakdown for small system sizes, since the number of peaks is already extremely low. Finally, in figure 2*d*, we analyse the average magnitude of spectral peaks, $\mu_{I_{\text{peak}}}$, as we shrink the frequency domain. Since the height of the peaks increases linearly with decreasing ϵ, we expect that $\mu_{I_{\text{peak}}}\epsilon$ is constant in the linear region. This holds approximately for larger system sizes, up to initial conditions at $\Omega \approx \Omega_0$. However, for smaller systems, and particularly $N_f = 6$, we see that the mean amplitude of the peaks fluctuates during the procedure, which shows that the influence of peak fluctuations and numerical noise is too great for a reliable scaling.

In general, structure factors for the Yukawa interaction are statistically self-similar with respect to frequency domain rescaling, for all values of screening. This is quantified by the linear scaling of their first two moments, as shown for $\lambda = 0$ in figure 2. However, since the mean and standard deviation of the structure factors approaches zero as $\lambda \to \infty$, as shown in figure 1, this self-similarity is most apparent for long-range interactions.

5. Discussion and conclusion

In this paper, we studied numerically the momentum-averaged dynamical density structure factors $I_{\bar{\rho}}$ (equation (3.8)) for the $\nu = 1/3$ Laughlin state on the torus, using the continued fraction method. Our main result is the discovery of a statistical self-similarity of the structure factor in the frequency domain. Specifically, in §4b, we showed that the peak distribution has fractal properties across several orders of magnitude. This self-similar nature is realized most precisely and across the largest range of frequency scales in the thermodynamic limit, for systems stabilized by long-range interactions. In addition, in §4a, we established the scaling behaviour of the structure factor with respect to interaction range. This dependence is determined by the asymptotic behaviour of the Yukawa interaction with respect to the screening parameter λ.

[7]The R^2 value is defined as the square of Pearson's correlation coefficient for the lines of best fit. Note that R^2 cannot be computed when the gradient $\kappa_\sigma \approx 0$.

Physically, the structure factor $I_{\bar{\rho}}(q_y, \omega)$, with q_y fixed, corresponds to the energy-resolved spectrum of particle excitations. The amplitudes and fine structure in the spectrum of peaks are consequently related to the probability distribution of many-particle excitations in the system. In §4a, we showed that an increase in the interaction range proportionally increases the centre and spread of particle excitations, which is a direct result of the increased average interaction amplitude, as well as the number of interaction permutations. Furthermore, in §4b, we demonstrated the fractality of the structure factors with respect to the energy axis, which reflects the continued chain of possible many-particle interactions with diminishing amplitudes, and is especially prevalent for systems stabilized by long-range interactions. Building on this, we expect that these properties also hold in the dynamical structure factors of other strongly correlated phases of matter with Coulomb-type interactions, such as superconductors [50] or transition metal oxides [51].

Our results highlight the effect of interaction range on, and the self-similarity of, dynamical structure factors $I_{\bar{\rho}}$ for FQH systems. However, statistical self-similarity is a more general property of response functions in condensed matter systems, and beyond. In particular, there have been a wealth of studies on the self-similarity, fractality and chaos of continued fractions in a mathematical context [19,20], and this is reflected in a wide class of observables derived from Green's function. We have explicitly demonstrated the fine structure of spectral response functions in the frequency domain, which stems in part from their continued fraction representation. This leaves scope for further manifestations of self-similarity due to this recurrence relation, as well as potential applications. For example, there is a natural limitation to the achievable energy resolution of structure factors derived from experiments, such as inelastic X-ray scattering and photoemission spectroscopies [52,53], which may be numerically enhanced using statistical interpolation. Moreover, dynamical quantum simulators have recently been proposed as a method to compute structure factors [54,55], which may be expedited using self-similarity relations. On a more pragmatic level, our results offer a way to efficiently approximate the Coulomb structure factor. Specifically, for systems stabilized with long-range interactions, the structure factor may be readily derived by diagonalizing a short-range Yukawa interaction Hamiltonian in Fourier space. Large λ yields a short-range interaction that is efficient to implement, and, provided the simulation resolution is sufficiently high, this result can be smoothly tuned to the long-range Coulomb limit.

To complement these results, in the electronic supplementary material, we examined the behaviour of dynamical structure factors for FQH states that are stabilized by Haldane pseudopotential interactions, which contrasts the effects of tuning the interaction range via the Yukawa mass, and truncating two-body interactions with large relative angular momenta. We showed that Haldane pseudopotentials are not designed to model long-range interactions on the torus at the system sizes currently accessible, however a reasonable approximation may be achieved, provided that the interactions are modulated to be sufficiently short-range relative to the system size. Using the example of the Coulomb structure factor from figure 1*b*, we found that the optimal approximation was recovered at pseudopotential order $\beta \sim N_\Phi/2$ with a weakly screened form of the interaction. This demonstrates that, provided sufficient care is taken, Haldane pseudopotentials provide another route to approximate dynamical structure factors for systems stabilized with long-range interactions, at a significantly reduced numerical cost.

There are several ways in which this work could be extended in the future. First, it would be interesting to build on this analysis of ground states in the same universality class at $\nu = 1/3$, to other FQH filling factors, and in particular, ground states that do not share a universality class and inherently require a long-range interaction to be stabilized [56,57]. Second, it would be useful to analyse the trade-off between interaction range/frequency window and simulation resolution using this approach to find the optimal efficiency benefit for a series of FQH states. Finally, there is current motivation to leverage this method and compute the full density-density response function, to identify collective excitations in FQH systems, and guide the latest experimental techniques, including spin wave spectroscopy in graphene [11].

Data accessibility. The functionality to compute spectral response functions for fractional quantum Hall states is available from the DiagHam repository: https://www.nick-ux.org/diagham/svn/DiagHam/. The scripts and data used for this manuscript are available from the Zenodo repository: https://doi.org/10.5281/zenodo.7991931.

Additional information is provided in the electronic supplementary material [58].

Authors' contributions. B.A.: data curation, formal analysis, funding acquisition, investigation, methodology, software, validation, visualization, writing—original draft, writing—review and editing; G.M.: conceptualization, funding acquisition, methodology, project administration, resources, software, supervision, writing—review and editing.

Both authors gave final approval for publication and agreed to be held accountable for the work performed therein.

Conflict of interest declaration. We declare we have no competing interests.

Funding. B.A. acknowledges support from the Swiss National Science Foundation under grant nos. P500PT_203168 and PP00P2_176877, as well as the University of California Laboratory Fees Research Program funded by the UC Office of the President (UCOP), grant no. LFR-20-653926. G.M. acknowledges support from the Royal Society under University Research Fellowship URF\R\180004.

Acknowledgements. We thank Garry Goldstein for help with the derivation of the momentum-averaged density operator, detailed in Sec. SIII of the electronic supplementary material. We thank Steve Simon, Nigel Cooper, Zlatko Papic, Nicholas Regnault, Kiryl Pakrouski, Titus Neupert and Jie Wang for useful discussions. Our numerical results were produced using DiagHam.

References

1. Girvin SM, MacDonald AH, Platzman PM. 1986 Magneto-roton theory of collective excitations in the fractional quantum Hall effect. *Phys. Rev. B* **33**, 2481–2494. (doi:10.1103/PhysRevB.33.2481)
2. Lopez A, Fradkin E. 1993 Response functions and spectrum of collective excitations of fractional-quantum-Hall-effect systems. *Phys. Rev. B* **47**, 7080–7094. (doi:10.1103/PhysRevB.47.7080)
3. Haussmann R. 1996 Electronic spectral function for a two-dimensional electron system in the fractional quantum Hall regime. *Phys. Rev. B* **53**, 7357–7375. (doi:10.1103/PhysRevB.53.7357)
4. Wójs A, Hawrylak P. 1997 Spectral functions of quantum dots in the integer and fractional quantum Hall regime. *Phys. Rev. B* **56**, 13 227–13 234. (doi:10.1103/PhysRevB.56.13227)
5. Repellin C, Neupert T, Papić Z, Regnault N. 2014 Single-mode approximation for fractional Chern insulators and the fractional quantum Hall effect on the torus. *Phys. Rev. B* **90**, 045114. (doi:10.1103/PhysRevB.90.045114)
6. Wang J, Geraedts SD, Rezayi EH, Haldane FDM. 2019 Lattice Monte Carlo for quantum Hall states on a torus. *Phys. Rev. B* **99**, 125123. (doi:10.1103/PhysRevB.99.125123)
7. Golkar S, Nguyen DX, Son DT. 2016 Spectral sum rules and magneto-roton as emergent graviton in fractional quantum Hall effect. *J. High Energy Phys.* **2016**, 21. (doi:10.1007/JHEP01(2016)021)
8. Liou S-F, Haldane FDM, Yang K, Rezayi EH. 2019 Chiral gravitons in fractional quantum Hall liquids. *Phys. Rev. Lett.* **123**, 146801. (doi:10.1103/PhysRevLett.123.146801)
9. Koch E. 2011 The Lanczos method. In *The LDA+DMFT approach to strongly correlated materials* (eds E Pavarini, E Koch, A Lichtenstein, D Vollhardt). Schriften des Forschungszentrums Jülich. Reihe Modeling and Simulation, vol. 1. Jülich: Forschungszenrum Jülich GmbH Zentralbibliothek, Verlag. (Chapter 8, p. getr. Zählung, record converted from VDB: 12.11.2012).
10. Kukushkin IV, Smet JH, Scarola VW, Umansky V, von Klitzing K. 2009 Dispersion of the excitations of fractional quantum Hall states. *Science* **324**, 1044–1047. (doi:10.1126/science.1171472)
11. Wei DS, van der Sar T, Lee SH, Watanabe K, Taniguchi T, Halperin BI, Yacoby A. 2018 Electrical generation and detection of spin waves in a quantum Hall ferromagnet. *Science* **362**, 229–233. (doi:10.1126/science.aar4061)
12. Nguyen DX, Son DT. 2021 Probing the spin structure of the fractional quantum Hall magnetoroton with polarized Raman scattering. *Phys. Rev. Res.* **3**, 023040. (doi:10.1103/PhysRevResearch.3.023040)

13. Kumar P, Haldane FDM. 2022 Neutral excitations of quantum Hall states: a density matrix renormalization group study. *Phys. Rev. B* **106**, 075116. (doi:10.1103/PhysRevB.106.075116)
14. Nguyen DX, Haldane FDM, Rezayi EH, Son DT, Yang K. 2022 Multiple magnetorotons and spectral sum rules in fractional quantum Hall systems. *Phys. Rev. Lett.* **128**, 246402. (doi:10.1103/PhysRevLett.128.246402)
15. Balram AC, Liu Z, Gromov A, Papić Z. 2022 Very-high-energy collective states of partons in fractional quantum Hall liquids. *Phys. Rev. X* **12**, 021008. (doi:10.1103/PhysRevX.12.021008)
16. Yuzhu W, Bo Y. 2023 Geometric fluctuation of conformal Hilbert spaces and multiple graviton modes in fractional quantum Hall effect. *Nat. Commun.* **14**, 2317. (doi:10.1038/s41467-023-38036-0)
17. Kumar P, Haldane FDM. 2023 A numerical study of bounds in the correlations of fractional quantum Hall states. (https://arxiv.org/abs/2304.14991)
18. Saarela M. 1987 Density-density response function in the fractional quantum Hall effect. *Phys. Rev. B* **35**, 854–856. (doi:10.1103/PhysRevB.35.854)
19. Obata S, Ohkuro S. 1999 Distribution phenomena in continued fractions and logistic map. *Prog. Theor. Phys.* **101**, 831–846. (doi:10.1143/PTP.101.831)
20. Obata S, Ohkuro S, Maeda T. 1999 Chaotic and chaos-like behavior in continued fractions. *Prog. Theor. Phys.* **101**, 1175–1179. (doi:10.1143/PTP.101.1175)
21. Keski-Vakkuri E, Wen X-G. 1993 The ground state structure and modular transformations of fractional quantum Hall states on a torus. *Int. J. Mod. Phys. B* **7**, 4227–4259. (doi:10.1142/S0217979293003644)
22. Li D. 1993 Hierarchical wave functions and fractional statistics in fractional quantum Hall effect on the torus. *Int. J. Mod. Phys. B* **7**, 2779–2794. (doi:10.1142/S0217979293003036)
23. He S, Simon SH, Halperin BI. 1994 Response function of the fractional quantized Hall state on a sphere. II. Exact diagonalization. *Phys. Rev. B* **50**, 1823–1831. (doi:10.1103/PhysRevB.50.1823)
24. Pakrouski K. 2017 Fractional quantum Hall effect and quantum spin Hall effect in semiconductor heterostructures. PhD thesis, ETH Zurich. (doi:10.3929/ethz-b-000164856)
25. Fremling M. 2015 Quantum Hall wave functions on a torus. PhD Thesis, Stockholm University.
26. Fremling M, Moran N, Slingerland JK, Simon SH. 2018 Trial wave functions for a composite Fermi liquid on a torus. *Phys. Rev. B* **97**, 035149. (doi:10.1103/PhysRevB.97.035149)
27. Repellin C, Neupert T, Bernevig BA, Regnault N. 2015 Projective construction of the $\mathbb{Z}_k$ Read-Rezayi fractional quantum Hall states and their excitations on the torus geometry. *Phys. Rev. B* **92**, 115128. (doi:10.1103/PhysRevB.92.115128)
28. Pu S, Wu Y-H, Jain JK. 2017 Composite fermions on a torus. *Phys. Rev. B* **96**, 195302. (doi:10.1103/PhysRevB.96.195302)
29. Pu S, Jain JK. 2021 Composite anyons on a torus. *Phys. Rev. B* **104**, 115135. (doi:10.1103/PhysRevB.104.115135)
30. Bai Z, Demmel J, Dongarra J, Ruhe A, van der Vorst H. 2000 *Templates for the Solution of Algebraic Eigenvalue Problems*. Philadelphia, PA: Society for Industrial and Applied Mathematics.
31. Dargel PE, Wöllert A, Honecker A, McCulloch IP, Schollwöck U, Pruschke T. 2012 Lanczos algorithm with matrix product states for dynamical correlation functions. *Phys. Rev. B* **85**, 205119. (doi:10.1103/PhysRevB.85.205119)
32. Haydock R, Heine V, Kelly MJ. 1972 Electronic structure based on the local atomic environment for tight-binding bands. *J. Phys. C: Solid State Phys.* **5**, 2845–2858. (doi:10.1088/0022-3719/5/20/004)
33. Haydock R, Heine V, Kelly MJ. 1975 Electronic structure based on the local atomic environment for tight-binding bands. II. *J. Phys. C: Solid State Phys.* **8**, 2591–2605. (doi:10.1088/0022-3719/8/16/011)
34. Heine V. 1980 Electronic structure from the point of view of the local atomic environment. *Solid State Phys.* **35**, 1. (doi:10.1016/S0081-1947(08)60503-2)
35. Bullett D. 1980 The renaissance and quantitative development of the tight-binding method. *Solid State Phys.* **35**, 129. (doi:10.1016/S0081-1947(08)60504-4)
36. Haydock R. 1980 The recursive solution of the Schrödinger equation. *Solid State Phys.* **35**, 215. (doi:10.1016/S0081-1947(08)60505-6)
37. Kelly M. 1980 Applications of the recursion method to the electronic structure from an atomic point of view. *Solid State Phys.* **35**, 295. (doi:10.1016/S0081-1947(08)60506-8)

38. Wietek A, Läuchli AM. 2018 Sublattice coding algorithm and distributed memory parallelization for large-scale exact diagonalizations of quantum many-body systems. *Phys. Rev. E* **98**, 033309. (doi:10.1103/PhysRevE.98.033309)
39. Andrews B, Möller G. 2018 Stability of fractional Chern insulators in the effective continuum limit of Harper-Hofstadter bands with Chern number $|C| > 1$. *Phys. Rev. B* **97**, 035159. (doi:10.1103/PhysRevB.97.035159)
40. Andrews B. 2019 Stability of topological states and crystalline solids. PhD thesis, University of Cambridge. (doi:10.17863/CAM.36140)
41. Hofstadter DR. 1976 Energy levels and wave functions of Bloch electrons in rational and irrational magnetic fields. *Phys. Rev. B* **14**, 2239–2249. (doi:10.1103/PhysRevB.14.2239)
42. Haldane FDM. 1983 Fractional quantization of the Hall effect: a hierarchy of incompressible quantum fluid states. *Phys. Rev. Lett.* **51**, 605–608. (doi:10.1103/PhysRevLett.51.605)
43. Weron A, Burnecki K, Mercik S, Weron K. 2005 Complete description of all self-similar models driven by Lévy stable noise. *Phys. Rev. E* **71**, 016113. (doi:10.1103/PhysRevE.71.016113)
44. Hastings HM, Sugihara G. 1993 *Fractals. A user's guide for the natural sciences*. Oxford, UK: Oxford University Press.
45. Falconer K. 2014 *Fractal geometry: mathematical foundations and applications*. 3rd edn. San Francisco, CA: Wiley.
46. Embrechts P, Maejima M. 2000 An introduction to the theory of self-similar stochastic processes. *Int. J. Mod. Phys. B* **14**, 1399. (doi:10.1142/S0217979200001047)
47. Peng C-K, Hausdorff JM, Goldberger AL. 2000 Fractal mechanisms in neuronal control: human heartbeat and gait dynamics in health and disease. In *Self-organized biological dynamics and nonlinear control: toward understanding complexity, chaos and emergent function in living systems* (ed J Walleczek), pp. 66–96. Cambridge, UK: Cambridge University Press. (doi:10.1017/CBO9780511535338.006)
48. Mandelbrot B, Hudson R. 2006 *The (mis)behaviour of markets: a fractal view of financial turbulence*. New York City, NY: Basic Books.
49. Andrews B, Möller G. 2023 Supplemental Data for 'Self-similarity of spectral response functions for fractional quantum Hall states'. Zenodo Dataset. (doi:10.5281/zenodo.7991931)
50. Dutta A, Bhattacharjee JK. 2013 Dynamical structure factor of Fulde-Ferrell-Larkin-Ovchinnikov superconductors. *AIP Conf. Proc.* **1512**, 1128. (doi:10.1063/1.4791444)
51. Gautreau DM, Saha A, Birol T. 2021 First-principles characterization of the magnetic properties of $Cu_2(OH)_3Br$. *Phys. Rev. Mater.* **5**, 024407. (doi:10.1103/PhysRevMaterials.5.024407)
52. Seidu A, Marini A, Gatti M. 2018 Dynamical correlation effects in a weakly correlated material: inelastic X-ray scattering and photoemission spectra of beryllium. *Phys. Rev. B* **97**, 125144. (doi:10.1103/PhysRevB.97.125144)
53. Ruotsalainen K, Nicolaou A, Sahle CJ, Efimenko A, Ablett JM, Rueff J-P, Prabhakaran D, Gatti M. 2021 Dynamical screening in $SrVO_3$: inelastic X-ray scattering experiments and *ab initio* calculations. *Phys. Rev. B* **103**, 235136. (doi:10.1103/PhysRevB.103.235136)
54. Baez ML, Goihl M, Haferkamp J, Bermejo-Vega J, Gluza M, Eisert J. 2020 Dynamical structure factors of dynamical quantum simulators. *Proc. Natl Acad. Sci. USA* **117**, 26 123–26 134. (doi:10.1073/pnas.2006103117)
55. Sun J, Vilchez-Estevez L, Vedral V, Boothroyd AT, Kim MS. 2023 Probing spectral features of quantum many-body systems with quantum simulators. (https://arxiv.org/abs/2305.07649)
56. Yang B, Wu Y-H, Papić Z. 2019 Effective Abelian theory from a non-Abelian topological order in the $\nu = 2/5$ fractional quantum Hall effect. *Phys. Rev. B* **100**, 245303. (doi:10.1103/PhysRevB.100.245303)
57. Andrews B, Mohan M, Neupert T. 2021 Abelian topological order of $\nu = 2/5$ and $3/7$ fractional quantum Hall states in lattice models. *Phys. Rev. B* **103**, 075132. (doi:10.1103/PhysRevB.103.075132)
58. Andrews M, Möller G. 2023 Self-similarity of spectral response functions for fractional quantum Hall states. Figshare. (doi:10.6084/m9.figshare.c.6742498)